Hadronic backgrounds through gamma-gamma collisions in a 5 TeV e^+e^- linear collider

T. Ohgaki and M. Xie
Lawrence Berkeley National Laboratory, Berkeley, California 94720
(May 1999)

We have estimated the hadronic backgrounds by $\gamma\gamma$ collisions in an e^+e^- linear collider at a center-of-mass energy of 5 TeV. We introduce a simple ansatz, that is, a $\gamma\gamma$ minijets cross section of $\sigma_{\rm jets'} = \sigma_{\rm tot} - \sigma_{\rm VMD}$ shall be saturated by minijet production, whose rate is controlled by $p_{t,min}(\sqrt{s})$. We present that the background yields are small and the energy deposits are tinier than the collision energy of the initial electron and positron beams by a simulation.

I. INTRODUCTION

A combination of beamstrahlung and 'strong' QCD interactions of the photon can induce hadronic backgrounds at future e^+e^- linear colliders. An operation of the e^+e^- linear collider at a center-of-mass energy of 5 TeV beyond the Large Hadron Collider and the 500 GeV e^+e^- linear collider requires a luminosity of $10^{35}{\rm cm}^{-2}{\rm s}^{-1}$ for a study of particle physics. In order to achieve the required luminosity in several TeV colliders, we need to more strongly focus the electron and positron beams at the interaction point. In the circumstance, a large number of beamstrahlung photons are radiated due to the collective electromagnetic field of the oncoming beam bunch. Some of collisions between them convert to e^+e^- pairs and others generate hadrons.

At high energy, we can consider that the photon consists of the partons which are quarks and gluons, and the interactions among the partons in two-photon collisions can be calculated using perturbative QCD. The experiments at TRISTAN, first indicated that the jet production in two-photon interactions was dominated by the resolved processes [1,2]. Drees and Godbole called attention to the minijet backgrounds for future e^+e^- linear colliders [3], because the cross section of minijets, by the calculation method of the parton-parton scattering, rises very fast with energy. Recently, two measurements of $\gamma\gamma$ collisions at the CERN e^+e^- collider LEP exhibit the rising of the total cross section for $\gamma\gamma \to hadrons$ with energy [4,5]. The minijet cross sections for description of hadronic events have uncertainties at several TeV energy, related to the cutoff of transverse momentum of the jet, $p_{t,min}$, such as a free parameter. Below $p_{t,min}$, the perturbative QCD calculations fail altogether and the transition region between hard and soft processes is not well defined. In addition, the parton density functions of the photon for the minijet cross section are parameterized according to the experimental data at low energies. In consequence, we can not simply estimate the number of hadronic events in 5 TeV e^+e^- linear colliders by using these cross sections [6,7].

In general, $\gamma\gamma$ interactions are similar to hadron-hadron interactions at high energy. The total cross sections for pp and γp collisions have been measured at several TeV and hundred GeV, which are more larger than $\gamma\gamma$ experimental data, respectively [8] and are well described by the Regge theorem [9]. Therefore, we propose the simple model by taking a phenomenological approach. First, the cross section for vector meson dominance (VMD) parts in $\gamma\gamma$ collisions, $\sigma_{\rm VMD}$, is applied by the additive quark model [10] and the factorization theorem [11–14], and we estimate the number of hadronic events at a 5 TeV e^+e^- linear collider. Next, the simple ansatz, that the total cross section of $\gamma\gamma$ minijets is supposed as $\sigma_{jets'} = \sigma_{\rm tot} - \sigma_{\rm VMD}$, where $\sigma_{\rm tot}$ is the total hadronic cross sections for $\gamma\gamma$ collisions, is applied and we compute the spatial distribution for $\gamma\gamma$ minijets. The detailed information of the minijets from realistic simulations is used to remove the hadronic backgrounds effectively.

Until now the hadron production in $\gamma\gamma$ collisions as a backgrounds for e^+e^- linear colliders at $\sqrt{s}_{e^+e^-}$=0.5 and 1.0 TeV has been studied [1,11,15]. Recently the design study for 5 TeV linear colliders in the deep quantum beamstrahlung regime, for example, the laser driven e^+e^- linear colliders, has been started and it presents that the effects of quantum suppression of beamstrahlung due to the very short bunch length are effective [16,17]. In Sec. II, we calculate the luminosity distribution of $\gamma\gamma$ collisions at a 5 TeV e^+e^- linear collider in the deep quantum regime. In Sec. III, we describe the factorization theorem about the cross section for $\gamma\gamma$ collisions and the simple ansatz of $\gamma\gamma$ minijets. In Sec. IV, we estimate hadronic backgrounds in $\gamma\gamma$ collisions by a simulation.

II. LUMINOSITY DISTRIBUTION

In this section, we will describe the spectrum of the photon-photon luminosity in a 5 TeV e^+e^- linear collider. There are two processes for $\gamma\gamma$ collisions in e^+e^- colliders. Beamstrahlung is a synchrotron radiation induced by

the collective fields of the oncoming colliding beams. The average Upsilon parameter in a linear collider [18], which expresses the dependence of the beamstrahlung spectrum, is

$$\Upsilon = \frac{5}{6}\frac{N_e r_e^2 \gamma}{\alpha_{\rm em}\sigma_z(\sigma_x+\sigma_y)}, \tag{1}$$

where $\alpha_{\rm em}$ is the fine structure constant, N_e the number of particles per bunch, r_e the classical electron radius, γ the Lorentz factor of the beam, σ_z the rms bunch length, and σ_x, σ_y the transverse and vertical sizes of the bunch at the interaction point. In this paper, we use the beamstrahlung spectrum in the deep quantum beamstrahlung regime $\Upsilon \gg 1$, taking advantage of effects of quantum suppression of beamstrahlung [16,17]. The spectra of beamstrahlung photons in the high Υ regime were calculated by the numerical computation [19]. In order to perform more realistic calculation including disruption, multiple beamstrahlung, and pair creation, we have simulated the luminosity distribution by using the CAIN code, which is a Monte Carlo program of the beam-beam interactions in future linear colliders [20].

Virtual photons are emitted by the collisions of individual particles. The spectrum of the virtual photons from electron beams is given by the well-known equivalent photon approximation [15]

$$n_v(y) = \frac{\alpha_{\rm em}}{2\pi}\left(\frac{1+(1-y)^2}{y}\ln\left[\frac{(1-y)P_{\rm max}^2}{m_e^2 y^2}\right] - \frac{2(1-y)}{y}\right), \tag{2}$$

where y and $P_{\rm max}^2$ denote the energy fraction taken by the photon from the electron and the maximum photon virtuality and m_e the electron mass. In this article, the photon virtuality was restricted to $P_{\rm max}^2 = 0.01$ GeV^2 [15].

The beam parameters of an e^+e^- linear collider with the laser drive at $\sqrt{s}_{e^+e^-} = 5$ TeV are listed in Table I. The Υ parameter of the laser-driven e^+e^- collider is some hundreds, because σ_z is much smaller than that of conventional microwaves due to the typical wavelength of accelerating wakefield for laser wakefield acceleration, which is about 100 μm.

Figure 1 shows the luminosity distribution of a 5 TeV linear collider with $\Upsilon = 631$. The luminosity distribution of the e^+e^-, $e\gamma$, and $\gamma\gamma$ collisions in Fig. 1 have been calculated by using the CAIN code. The maximum energy of the collisions between beamstrahlung photons reaches near $\sqrt{s} = 5$ TeV due to the large Υ parameter. The luminosity of the $\gamma^*\gamma^*$ collisions (γ^* denotes virtual photons.) was calculated by

$$L_{\gamma^*\gamma^*}(\sqrt{s}) = L_{ee}\int_0^1\int_0^1 n_v(y_1)n_v(y_2)\delta\left(s - 4y_1y_2E_0^2\right)dy_1dy_2, \tag{3}$$

where E_0 is the energy of initial electrons and L_{ee} the total luminosity of the e^+e^- collisions, using the analytic formula of Eq.(2). The collisions between virtual photons over $\sqrt{s} > 1$ TeV is negligible in comparison with other collisions. It is needless to say that we will have to consider the superposition of the beamstrahlung and virtual photon spectrums.

The total luminosity of an e^+e^- linear collider with the laser drive at $\sqrt{s}_{e^+e^-} = 5$ TeV are listed in Table II. There is about a half of the total luminosity of the e^+e^- collisions with $\sqrt{s} > 4.975$ TeV and it presents a narrow width for precision study.

III. THE CROSS SECTION OF $\gamma\gamma$ MINIJETS

A. The total cross section of $\gamma\gamma$ collisions

1. The total cross section

In general, $\gamma\gamma$ interactions are similar to hadron-hadron interactions at high energy. The total cross sections for pp and γp collisions are well described by the Regge parameterization [8,9]

$$\sigma_{pp} = X_{pp}s^{\epsilon} + Y_{1pp}s^{-\eta_1} + Y_{2pp}s^{-\eta_2}\ \text{mb}, \tag{4}$$

$$\sigma_{\gamma p} = X_{\gamma p}s^{\epsilon} + Y_{1\gamma p}s^{-\eta_1}\ \text{mb}, \tag{5}$$

where s is the square of the center-of-mass energy of the interaction and is given in (GeV)^2. The exponents $\epsilon = 0.095$, $\eta_1 = 0.34$, and $\eta_2 = 0.55$ are independent of the particles [8]. The factors $X_{pp} = 18.304$, $Y_{1pp} = 60.12$, $Y_{2pp} = 32.84$,

$X_{\gamma p} = 0.0579$, and $Y_{1\gamma p} = 0.1170$ were fitted to the experimental data [8]. The first, second, and third terms in Eqs. (4) and (5) correspond to the Pomeron, and lower-lying C-even and C-odd exchanges, respectively. The Pomeron exchange gives the asymptotic rise of the cross section and the another terms represent the behavior of it at low energies. Due to the only C-even Reggeon exchange between the photon and the proton, the cross section for γp collisions has only two terms.

The fitting total cross section for $\gamma\gamma$ collisions is similarly described as [8]

$$\sigma_{\rm tot} = 156 s^{\epsilon} + 320 s^{-\eta_1} \text{ nb}. \tag{6}$$

The experimental data of the total cross section of $\gamma\gamma$ collisions [4,5,21] are shown in Fig 2. The observed energy dependence of the cross section of the L3 and OPAL measurements is similar, but the OPAL values are about 20% higher [5]. The $\sigma_{\rm tot}$ in Eq. (6) is derived from fitting these data except for the OPAL [8] and the $\sigma_{\rm tot}$ at higher energies suits to the L3 values.

The experimental data of pp collisions have been measured over $\sqrt{s} = 1$ TeV and the HERA measurements at DESY ep collider have accumulated the γp collisions at near $\sqrt{s} = 200$ GeV. The formulas in Eqs. (4) and (5) accommodate with these data. Here we introduce the cross section for $\gamma\gamma$ collisions by the following factorization theorem [12]

$$X_{\gamma\gamma} = \frac{(X_{\gamma p})^2}{X_{pp}}, \tag{7}$$

$$Y_{1\gamma\gamma} = \frac{(Y_{1\gamma p})^2}{Y_{1pp}}, \tag{8}$$

and we can derive the factorized total cross section for $\gamma\gamma$ collisions as

$$\sigma_{\rm tot'} = 183 s^{\epsilon} + 228 s^{-\eta_1} \text{ nb}. \tag{9}$$

The experimental data are compared to the $\sigma_{\rm tot}$ and the $\sigma_{\rm tot'}$ in Fig. 2 and the $\sigma_{\rm tot'}$ is about 10% larger than the $\sigma_{\rm tot}$. Since the difference between the $\sigma_{\rm tot}$ and the $\sigma_{\rm tot'}$ is small, we use the $\sigma_{\rm tot}$ as the total cross section for $\gamma\gamma$ collisions in the paper.

2. The VMD parts

According to the vector dominance model, the photon fluctuates into a vector meson (such as the ρ, ω, or ϕ)

$$\gamma \rightarrow V, \tag{10}$$

and this vector meson in turn couples to other hadrons. The total VMD cross sections of meson-proton interactions are in good agreement with experiments. Here we present the VMD cross section for $\gamma\gamma$ collisions using the additive quark model [10] and the factorization theorem.

The ρp, ωp, and ϕp cross sections are obtained by the additive quark model and the measurements in πp and Kp collisions [8,10,12]

$$\sigma_{\rho p} = \sigma_{\omega p} = \frac{\sigma_{\pi^+ p} + \sigma_{\pi^- p}}{2} = 11.594 s^{\epsilon} + 27.52 s^{-\eta_1} \text{ mb}, \tag{11}$$

$$\sigma_{\phi p} = \sigma_{K^+ p} + \sigma_{K^- p} - \sigma_{\pi^- p} = 9.112 s^{\epsilon} + 4.14 s^{-\eta_1} - 5.53 s^{-\eta_2} \text{ mb}. \tag{12}$$

More heavier mesons such as J/ψ are not included in this analysis, because the elastic photoproduction cross section of $\gamma p \rightarrow J/\psi p$ [22] is smaller than that of $\gamma p \rightarrow \rho p$ [23] by two order, and we take account of contributions from the three light vector mesons, ρ, ω, and ϕ.

The total cross section for two vector mesons is given by the factorization theorem

$$\sigma_{V_1 V_2} = \frac{X_{V_1 p} X_{V_2 p}}{X_{pp}} s^{\epsilon} + \frac{Y_{V_1 p} Y_{V_2 p}}{Y_{1pp}} s^{-\eta_1}, \tag{13}$$

where $V_i = \rho, \omega, \phi$ and the total VMD cross section may be written by

$$\sigma_{\rm VMD} = \sum_{V_1} \frac{4\pi\alpha_{\rm em}}{f_{V_1}^2} \sum_{V_2} \frac{4\pi\alpha_{\rm em}}{f_{V_2}^2} \sigma_{V_1 V_2}, \tag{14}$$

where the γ-meson coupling parameters $f_\rho^2/4\pi = 2.20$, $f_\omega^2/4\pi = 23.6$, and $f_\phi^2/4\pi = 18.4$ [24].

Finally, the total VMD cross section is given by

$$\sigma_{\rm VMD} = 114 s^{\epsilon} + 171 s^{-\eta_1} \text{ nb}. \tag{15}$$

From this assumption, we can predict that the ratio $\sigma_{\rm VMD}/\sigma_{\rm tot} \approx 0.73$ when $\sqrt{s} > 200$ GeV and the VMD parts dominate clearly.

3. The $\gamma\gamma$ minijets

A real photon has a complicated nature, and $\gamma\gamma$ events are divided into several event classes by the combinations of the nature of the two incoming photons [12]. The total cross section for $\gamma\gamma$ collisions is divided by

$$\sigma_{\rm tot} = \sigma_{\rm soft} + \sigma_{jets} = \sigma_{\rm soft} + \int_{p_{t,min}}^{\infty} \frac{d\sigma_{jets}}{dp_t}\, dp_t, \tag{16}$$

where σ_{jets} is the total cross section of $\gamma\gamma$ minijets. In lowest order, the minijet events consist of the 'direct' process $\gamma\gamma \to q\bar{q}$, the '1-resolved' processes $\gamma q \to q$g and γg $\to q\bar{q}$, and the '2-resolved' processes $qq' \to qq'$, $q\bar{q}' \to q\bar{q}'$, $q\bar{q} \to q'\bar{q}'$, $q\bar{q} \to$ gg, qg $\to qg$, gg $\to q\bar{q}$, and gg $\to$ gg. In general, the minijet cross section is infrared divergent and requires a cutoff at low transverse momentum. $\sigma_{\rm soft}$ is the total cross section of the soft vector meson dominance events which are the elastic, diffractive, and low-p_t events at $p_t < p_{t,min}$. At higher energies, the minijet events are increasing and the $\gamma\gamma$ minijet events with high p_t dominate in $\gamma\gamma$ hadronic backgrounds.

In order to estimate the number of $\gamma\gamma$ minijet events with high p_t, we propose the following relation

$$\sigma_{\rm tot} = \sigma_{\rm VMD} + \sigma_{jets'}, \tag{17}$$

where $\sigma_{jets'}$ is the minijet cross section with high p_t. In this assumption, we separate the non-perturbative part ($\sigma_{\rm VMD}$) and the perturbative QCD part ($\sigma_{jets'}$) from $\gamma\gamma$ events.

The minijet cross section with high p_t is given by

$$\begin{aligned} \sigma_{jets'} &= \sigma_{\rm tot} - \sigma_{\rm VMD} \\ &= 42 s^{\epsilon} + 149 s^{-\eta_1}, \end{aligned} \tag{18}$$

and the fraction $\sigma_{jets'}/\sigma_{\rm tot} \approx 0.27$ when $\sqrt{s} > 200$ GeV. Figure 3 shows the total, VMD, and minijet cross sections in $\gamma\gamma$ collisions.

B. The differential cross section of $\gamma\gamma$ minijets

We simply summarize the cross section of the $\gamma\gamma$ minijets [3,25,26]. In leading order (LO), the differential cross section for $\gamma\gamma$ minijets of two (partonic) jets with transverse momentum p_t and (pseudo) rapidities η_1, η_2 can be written as [26]

$$\frac{d^3\sigma_{mjets}(\gamma\gamma \to j_1 j_2 X)}{dp_t d\eta_1 d\eta_2} = 2p_t x_1 x_2 \sum_{i,j,k,l} f_{i|\gamma}(x_1) f_{j|\gamma}(x_2) \frac{d\hat{\sigma}_{ij\to kl}\left(\hat{s},\hat{t},\hat{u}\right)}{d\hat{t}}, \tag{19}$$

where i or j is a photon, quark or gluon, and k or l is a quark or gluon. Here $f_{i|\gamma}$ is the parton density function of the photon. If $i = \gamma$ (direct contribution), the function $f_{i|\gamma}$ is unity. x is the fraction of the jet energy carried by the parton in the photon. The subprocess cross sections $\hat{\sigma}$ for the direct and resolved photon contributions depend on the Mandelstam variables describing the hard partonic scattering, with $\hat{s} = x_1 x_2 s$ and $\hat{t}$ is described as [26]

$$\hat{t} = -\frac{\hat{s}}{2}\left(1 \pm \sqrt{1 - \frac{4p_t^2}{\hat{s}}}\right). \tag{20}$$

In order to grasp the behavior of the total cross section of $\gamma\gamma$ minijets at higher energies, we have computed several cross sections by the PDFLIB 7.09 [27] and PYTHIA 5.7 [28] codes. These total cross sections can be calculated including higher order effects by using the Monte Carlo codes. Figure 4 shows the cross sections of $\gamma\gamma$ minijets. The

parton density functions DG-G [29], LAC-1 [30], GS-G [31], AFG-G [32], and SaS-G 2M [33] have been calculated with $p_{t,min}$=2 GeV except for the function GRV-G [34] with $p_{t,min}$=3 GeV. The cross sections are compared to Chen's model [11] with $p_{t,min}$=3.2 GeV. The results of this figure show that the total cross sections of minijets almost rise very fast and are large at 5 TeV collision energy. It is known as the saturation problem of the photon density function at higher energies [6], and its problem does not depend on the parameterizations of the photon density function. Moreover the differences between the cross sections at higher energies greatly depend on the choice of $p_{t,min}$, such as a free parameter. Therefore we do not simply accept these minijet cross sections.

In order to evaluate the spatial distribution from minijet events, we must define the differential cross section of $\gamma\gamma$ minijets. Now we can not rely on the total cross sections of $\gamma\gamma$ minijets calculated by the present parton density functions of the photon at higher energies. Therefore we consider $\sigma_{jets'}$ in Eq.(18) as the upper bound of the minijet cross section. We obey this simple ansatz and the total cross section of $\gamma\gamma$ minijets is defined by

$$\sigma_{mjets}(p_{t,min}(\sqrt{s})) = \int_{p_{t,min}(\sqrt{s})}^{\infty} \frac{d\sigma_{mjets}}{dp_t}\, dp_t \equiv \sigma_{jets'}. \tag{21}$$

To satisfy the equality in Eq.(21), we change the parameter $p_{t,min}(\sqrt{s})$ according to each parton density function of the photon. The minimum of the transverse momentum $p_{t,min}$ is defined as

$$p_{t,min}(\sqrt{s}) = a \ln \sqrt{s/b}, \tag{22}$$

where a and b are the fitting coefficients given in GeV and $(\mathrm{GeV})^2$.

Table III lists the fitting coefficients a and b of the minimum of the transverse momentum $p_{t,min}$ which depends on each parton density function of the photon. The $p_{t,min}$ of the GS-G parameterization is similar to that of SaS-G 2M in the table. The minimum of the transverse momentum $p_{t,min}$ which depends on the parton density function of the photon are presented in Fig. 5. The LAC-1 parameterization is larger than others and about 17 GeV at $\sqrt{s}$=5 TeV. In the later section, we use the $p_{t,min}$ for estimation of hadronic backgrounds.

IV. TOTAL NUMBER OF EVENTS OF HADRONIC PRODUCTION IN $\gamma\gamma$ COLLISIONS

In this section, we consider the number of the $\gamma\gamma \to hadrons$ events taking account of the luminosity distribution in $\gamma\gamma$ collisions. Figure 6 shows the events of $\gamma\gamma \to hadrons$ per bunch crossing. Number of events of $\gamma\gamma \to hadrons$, VMD, and minijets per bunch crossing are listed in Table IV. From the figure and the table, the hadronic backgrounds from virtual photons are small at TeV energy as compared with those from beamstrahlung photons with $\Upsilon = 631$. Here we consider that the probability to have an event without background is $P_{clean} \equiv e^{-<n>}$, where $< n >$ is the average number of background events. When $< n >= 1.6 \times 10^{-2}$ from collisions between beamstrahlung photons in the range 1 TeV $< \sqrt{s} <$ 5 TeV in the table, $P_{clean} = 0.984$. It presents that the number of hadronic backgrounds with the energy 1 TeV $< \sqrt{s} <$ 5 TeV per bunch crossing is small so that it will not affect the performance of the detection in a study of particle physics. The number of events per bunch is inversely proportional to the collision frequency, because the luminosity per bunch is $L_{bunch} = L_{total}/f_c$. In this paper, the collision frequency of 5 TeV e^+e^- linear collider with the laser drive is 156 kHz and is higher than the frequency 120×225 Hz with 34 GHz normal conducting RF [35]. Until now the bunch scheme of the laser-driven linear collider is not well studied. We further need to estimate the number of hadronic backgrounds taking account of the bunch scheme of the laser-driven linear colliders.

V. RESULTS OF SIMULATION

In the previous section, we have estimated the number of minijet backgrounds per bunch crossing, but the number relies on the fitting formula in Eq.(6) and the bunch scheme of the laser-driven linear colliders is not well-known. If we grasp the spatial distribution of $\gamma\gamma$ minijets, we can remove the hadronic backgrounds effectively. By the detailed information of the visible energy and the transverse momentum, and so on of the jets from realistic simulations, we can reach near the probability $P_{clean} = 1$ which means that there are no hadronic backgrounds. To generate hadronic backgrounds, first we have calculated the realistic luminosity distribution of $\gamma\gamma$ collisions from beamstrahlung photons by a Monte Carlo simulation program CAIN. The luminosity distribution is described by two dimension of normalized cms energy $z = \sqrt{s}/(2E_0)$ and rapidity $\eta = \ln \sqrt{w_1/w_2}$ in order to take account of collisions between photons of unequal energy. Here w_1 and w_2 are the energies of left- and right-moving photons.

To represent the spatial distribution from minijet events, we use the parton distribution function of Drees and Grassie (DG-G) [29] for the photon by way of example. Because the saturation problem does not depend on the parameterizations of the photon density function as seen in the previous section. Here a cutoff $p_{t,min}$ for the DG-G parameterization in the previous section have been taken as

$$p_{t,min}(\sqrt{s}) = \begin{cases} 2.9 \ln \sqrt{s/12000} \text{ GeV} & \sqrt{s} > 366 \text{ GeV} \\ 3.5 \text{ GeV} & \sqrt{s} \leq 366 \text{ GeV} \end{cases} , \tag{23}$$

where s is given in $(\text{GeV})^2$. Here the minimum of $p_{t,min}$ is assumed as 3.5 GeV, because we keep away from $p_{t,min} < 0$ and get the calm transition.

The subprocess cross sections in Eq.(19) have been calculated by using the PYTHIA 5.7 code. Subsequent hadronizations of minijets are simulated by the parton shower picture with the JETSET 7.3. In this analysis, the JLC-I detector simulator [36] is applied for selection performances in the JLC-I detector which has the acceptance $|\cos\theta| < 0.95$ [36]. The main components used in this simulator are the central drift chamber and calorimeters.

Figure 7 shows the distribution of the visible energy and the transverse momentum of the tracking detector and calorimeters. The number of generated events is 50000 and the event number in the histogram of Fig. 7 corresponds to an integrated luminosity of 0.1 pb^{-1}. The 27% of all generated events are missed in the detector as shown by the peak. The deposits of the visible energy of the calorimeters are nearly below 200 GeV and the transverse momentum of the tracking detector above 40 GeV almost never has been seen.

The average visible energy and transverse momentum of the tracking detector and calorimeters per event are listed in Table V. The energy deposits per event are more smaller than the 5 TeV collision energy of initial electron and positron beams. The simulation results on hadronic backgrounds at the 0.5 and 1 TeV Next Linear Collider [11] presented small energy depositions which are similar to our results. Since the particles from minijets will deposit most of their energy inside the mask. According to the table, it is shown that the selection by applying the cut of the visible energy and the transverse momentum greatly reduces the hadronic backgrounds.

VI. SUMMARY AND CONCLUSIONS

We have estimated the hadronic backgrounds by $\gamma\gamma$ collisions in an e^+e^- collider at a center-of-mass energy of 5 TeV. The e^+e^- linear collider based on the laser driven acceleration is adopted taking advantage of effects of quantum suppression of beamstrahlung. The assumption that the behavior of the total cross section of $\gamma\gamma$ collisions is similar to that of hadronic interactions at high energy is applied, because the assumption gives a reasonable description of the total cross section for $\gamma\gamma$ collisions as compared with experimental data. The number of hadronic backgrounds per bunch crossing is small so that it will not affect the performance of the detection in a study of elementary particle physics. Further we need to estimate the number of hadronic backgrounds taking account of the bunch scheme of the laser-driven linear colliders.

We have calculated the total cross sections of $\gamma\gamma$ minijets depended on the parton density function of the photon with the fixed minimum of transverse momentum and the results show the ambiguities on minijet cross sections at higher energy, related to the cutoff of transverse momentum. Therefore we propose the simple model for minijets by taking a phenomenological approach.

First, the simple ansatz that the total cross section of $\gamma\gamma$ minijets is supposed as $\sigma_{jets'} = \sigma_{\text{tot}} - \sigma_{\text{VMD}}$, is applied as the upper bound of the minijet cross section. In order to evaluate the spatial distribution from minijet events, first we have calculated the fitting functions of the minimum transverse momentum, $p_{t,min}(\sqrt{s})$, which are depended on the photon parton distributions DG-G, LAC-1, GS-G, GRV-G, AFG-G, and SaS 2M by the PDFLIB 7.09 code on the assumption of the ansatz.

By using the fitting function of the minimum transverse momentum on the DG-G parameterization, we have performed the detector simulation. The detailed information of the minijets from realistic simulations is used to remove the hadronic backgrounds effectively. The Monte Carlo programs CAIN, PYTHIA 5.7, JETSET 7.3, and JLC-I detector simulator are applied for a 2-dimensional luminosity distribution of $\gamma\gamma$ collisions, the cross section of $\gamma\gamma$ minijets, hadronizations, and selection performances in the detector, respectively. The results show that the energy deposits per event are more smaller than the 5 TeV collision energy of the initial electron and positron beams.

ACKNOWLEDGMENTS

We wish to extend many thanks to M.M. Block, S. Chattopadhyay, P. Chen, L. Dixon, R.M. Godbole, T. Markiewicz, H. Murayama, M. Peskin, M. Ronan, J. Siegrist, T. Sjöstrand, T. Takahashi, T. Tauchi, and K. Yokoya for helpful discussions. This work was supported in part by the U.S. Department of Energy under Contract No. DE-AC03-76SF00098.

TABLE I. Beam parameters of an e^+e^- linear collider with the laser drive at $\sqrt{s}_{e^+e^-}$=5 TeV [16].

Υ	P_b (MW)	$N_e(10^8)$	f_c (kHz)	ϵ_x/ϵ_y (nm)	$\beta_x/\beta_y(\mu$m)	σ_x/σ_y (nm)	σ_z (μm)
631	20	1.6	156	25/25	62/62	0.56/0.56	1

TABLE II. Total luminosity of an e^+e^- linear collider with the laser drive at $\sqrt{s}_{e^+e^-}$=5 TeV (Unit 10^{35}cm^{-2}s^{-1}).

	L_{ee}	L_{ee} ($\sqrt{s} > 4.975$ TeV)	$L_{e\gamma}$	$L_{\gamma\gamma}$	$L_{\gamma^*\gamma^*}$ ($\sqrt{s}$ >1 GeV)
Total	1.3	0.61	0.49	0.21	0.34

TABLE III. The fitting coefficients a and b of the minimum of the transverse momentum $p_{t,min}$ which depends on the parton density function of the photon. There are the sets of leading order (LO) and next-to-leading logarithmic (NLL) evolutions.

Parton Density Function	Order of α_s	a (GeV)	b (GeV)^2
DG-G Set 1	LO	2.9	12000
LAC-G Set 1	LO	4.6	11000
GS-G-96 HO	NLL	1.9	6400
GRV-G	LO	2.4	6500
AFG-G Set HO	NLL	1.6	2600
SaS-G 2M	LO	1.9	6800

TABLE IV. Number of events of $\gamma\gamma \to hadrons$ per bunch crossing in the cms energy regions of (a) 1 GeV< $\sqrt{s}$ <5 TeV and (b) 1 TeV< $\sqrt{s}$ <5 TeV.

	Beamstrahlung		Virtual photons	
	(a)	(b)	(a)	(b)
Total	6.5×10^{-2}	1.6×10^{-2}	1.1×10^{-1}	9.7×10^{-4}
VMD	4.5×10^{-2}	1.2×10^{-2}	7.0×10^{-2}	7.1×10^{-4}
Minijet	2.0×10^{-2}	4.3×10^{-3}	4.3×10^{-2}	2.6×10^{-4}

TABLE V. The average visible energy and transverse momentum per event.

Tracking Detector		Calorimeters	
E_{vis} (GeV)	P_t (GeV)	E_{vis} (GeV)	P_t (GeV)
10	6.0	50	19

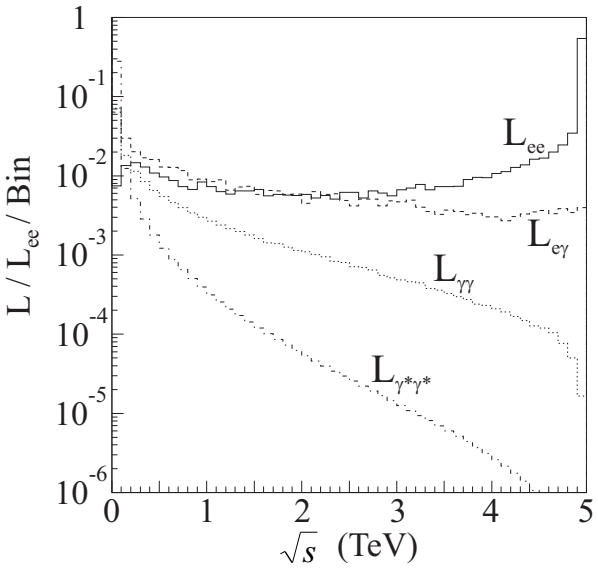

FIG. 1. Luminosity distribution of a 5 TeV e^+e^- linear collider with $\Upsilon = 631$. The vertical axis is normalized by the total luminosity of the e^+e^- collisions. The bin size is 100 GeV.

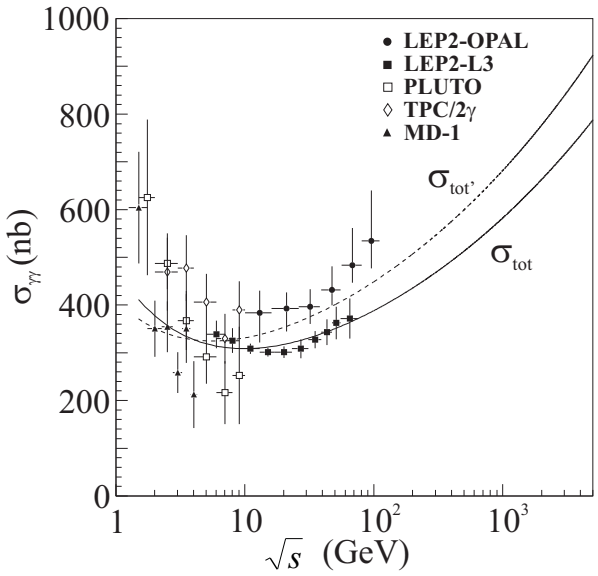

FIG. 2. The experimental data of the total cross section of $\gamma\gamma$ collisions. The measurements by PLUTO, TPC/2γ, MD1,L3, and OPAL are shown [4,5,21]. The data are compared to the $\sigma_{\rm tot}$ and the $\sigma_{\rm tot'}$.

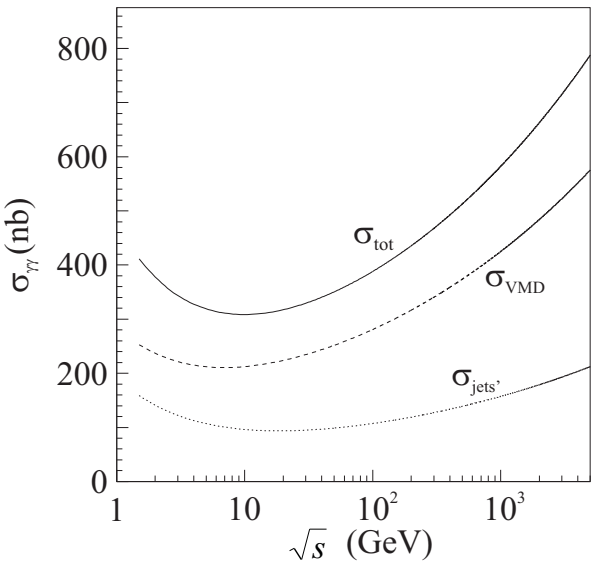

FIG. 3. The total, VMD, and minijet cross sections in $\gamma\gamma$ collisions.

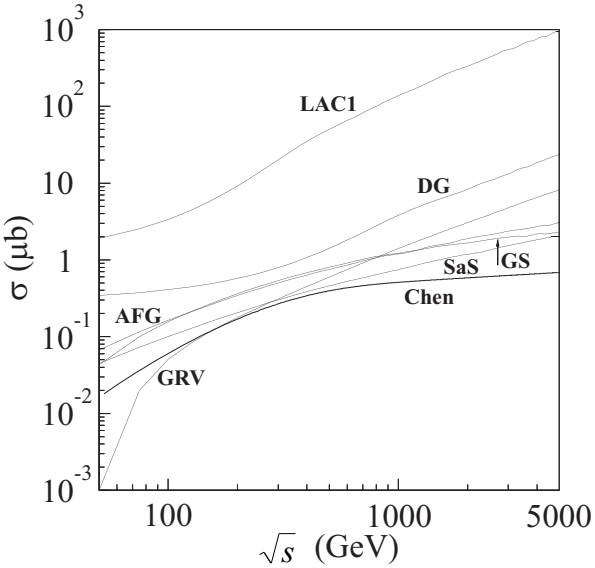

FIG. 4. The cross sections of $\gamma\gamma$ minijets. Computed by the PDFLIB 7.09 [27] and PYTHIA 5.7 [28] codes. The parton density functions have been calculated with $p_{t,min} = 2$ GeV except for the function GRV-G with $p_{t,min} = 3$ GeV. The cross sections are compared to Chen's model [11] with $p_{t,min} = 3.2$ GeV.

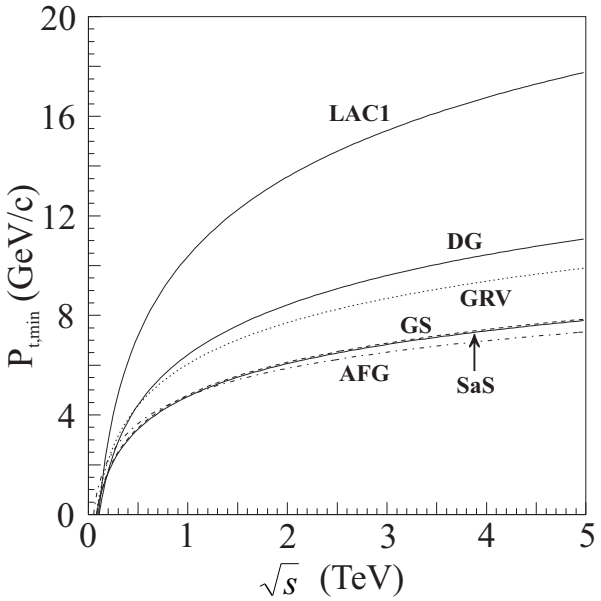

FIG. 5. The minimum of the transverse momentum $p_{t,min}$ which depends on the parton density function of the photon.

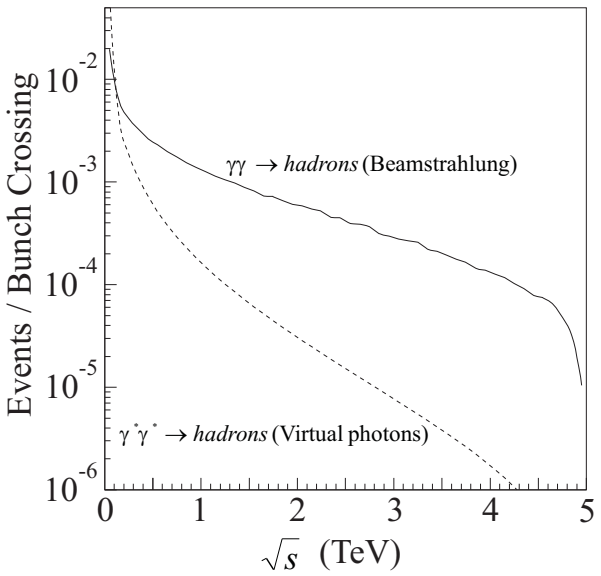

FIG. 6. The events of $\gamma\gamma \rightarrow hadrons$ per bunch crossing.

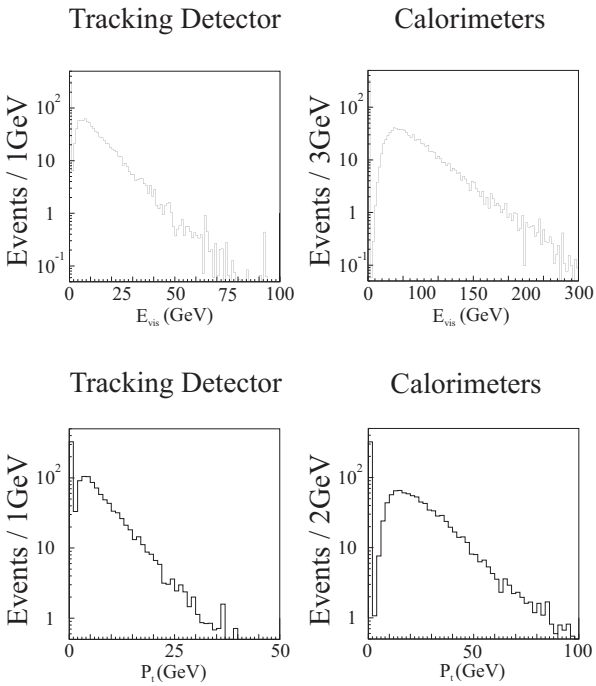

FIG. 7. The distribution of the visible energy and the transverse momentum of the tracking detector and calorimeters. The number of events corresponds to an integrated luminosity of 0.1 pb^{-1}.

---

[1] T. Tauchi and H. Hayashii, in *Proceedings of the Workshop on Physics and Experiments with Linear e^+e^- Colliders*, Waikoloa, Hawaii, 26-30 Apr 1993.

[2] TOPAZ Collaboration, H. Hayashii *et al.*, Phys. Lett. B **314**, 149 (1993); AMY Collaboration, B.J. Kim *et al.*, Phys. Lett. B **325**, 248 (1994).

[3] M. Drees and R.M. Godbole, Phys. Rev. Lett. **67**, 1189 (1991).

[4] L3 Collaboration, M. Acciarri *et al.*, Phys. Lett. B **408**, 450 (1997).

[5] F. Wäckerle, Nucl. Phys. Proc. Suppl. **71**, 381 (1999); S. Söldner-Rembold, Talk given at *the 18th International Symposium on Lepton-Photon Interactions*, Hamburg, Germany, 28 Jul-1 Aug 1997.

[6] R.M. Godbole, in *Proceedings of the 15th ICFA Advanced Beam Dynamics Workshop on Quantum Aspects of Beam Physics*, Monterey, CA, 4-9 Jan 1998.

[7] T. Ohgaki, in *Proceedings of the 15th ICFA Advanced Beam Dynamics Workshop on Quantum Aspects of Beam Physics*, Monterey, CA, 4-9 Jan 1998; T. Ohgaki, in *Proceedings of the 8th Workshop on Advanced Accelerator Concepts*, Baltimore, MD, 5-11 Jul 1998.

[8] Particle Data Group, Review of Particle Physics, Eur. Phys. J. C **3**, 1 (1998).

[9] A. Donnachie and P.V. Landshoff, Phys. Lett. B **296**, 227 (1992).

[10] E.M. Levin and L.L.Frankfurt, JETP Lett. **2**, 65 (1965); H.J. Lipkin and F. Scheck, Phys. Rev. Lett. **16**, 71 (1966); H. Joos, Phys. Lett. **24B**, 103 (1967).

[11] P. Chen, T.L. Barklow, and M.E. Peskin, Phys. Rev. D **49**, 3209 (1994).

[12] G.A. Schuler and T. Sjöstrand, Z. Phys. C **73**, 677 (1997).

[13] M.M. Block, E.M. Gregores, F. Halzen, G. Pancheri, Phys. Rev. D **58**, 017503 (1998).

[14] M.M. Block, E.M. Gregores, F. Halzen, G. Pancheri, MADPH-98-1041 (1998).

[15] R. Engel and J. Ranft, Phys. Rev. D **54**, 4244 (1996).

[16] M. Xie, T. Tajima, K. Yokoya, and S. Chattopadhyay, in *Proceedings of the 7th Workshop on Advanced Accelerator Concepts*, Lake Tahoe, CA, 13-19 Oct 1996.

[17] M. Xie, in *Proceedings of the 15th ICFA Advanced Beam Dynamics Workshop on Quantum Aspects of Beam Physics*, Monterey, CA, 4-9 Jan 1998; M. Xie, in *Proceedings of the 8th Workshop on Advanced Accelerator Concepts*, Baltimore, MD, 5-11 Jul 1998.

[18] K. Yokoya and P. Chen, in *Frontiers of Particle Beams: Intensity Limitations, Lecture Notes* in Physics Vol. 400 (Springer-

Verlag, Berlin, 1992).
[19] R.J. Noble, Nucl. Instrum. and Methods Phys. Res. A **256**, 427 (1987).
[20] P. Chen, T. Ohgaki, A. Spitkovsky, T. Takahashi, and K. Yokoya, Nucl. Instrum. and Methods Phys. Res. A **397**, 458 (1997).
[21] PLUTO Collaboration, Ch. Berger *et al.*, Phys. Lett. **149B**, 421 (1984) ; TPC/2γ Collaboration, H. Aihara *et al.*, Phys. Rev. D **41**, 2667 (1990) ; MD1 Collaboration, S.E. Baru *et al.*, Z. Phys. C **53**, 219 (1992).
[22] ZEUS Collaboration, M. Derrick *el al.*, Phys. Lett. B **350**, 120 (1995); H1 Collaboration, S. Aid *et al.*, Nucl. Phys. B **472**, 3 (1996).
[23] ZEUS Collaboration, M. Derrick *el al.*, Z. Phys. C **69**, 39 (1995); H1 Collaboration, S. Aid *et al.*, Nucl. Phys. B **463**, 3 (1996).
[24] T.H. Bauer *et al.*, Rev. Mod. Phys. **50**, 261 (1978).
[25] M. Drees and F. Halzen, Phys. Rev. Lett. **61**, 275 (1988).
[26] M. Drees and R.M. Godbole, J. Phys. G **21**, 1559 (1995).
[27] H. Plothow-Besch,"*PDFLIB: Nucleon, Pion, and Photon Parton Density Functions and α_s Calculations*", Users's Manual - Version 7.09, W5051 PDFLIB, 1997.07.02, CERN-PPE.
[28] T. Sjöstrand, Comput. Phys. Commun. **82**, 74 (1994).
[29] M. Drees and K. Grassie, Z. Phys. C **28**, 451 (1985).
[30] H. Abramowicz, K. Charchula, and A. Levy, Phys. Lett. B **269**, 458 (1991).
[31] L.E. Gordon and J.K. Storrow, Nucl. Phys. B **489**, 405 (1997).
[32] P. Aurenche, J.P. Guillet, and M. Fontannaz, Z. Phys. C **64**, 621 (1994).
[33] G.A. Schuler and T. Sjöstrand, Z. Phys. C **68**, 607 (1995).
[34] M. Glück, E. Reya, and A. Vogt, Phys. Rev. D **46**, 1973 (1992).
[35] S. Chattopadhyay *et al.*, in *Proceedings of the 1996 DPF/DPB Summer Study on New Directions for High-Energy Physics* (Snowmass 96), Snowmass, CO, 25 Jun-12 Jul 1996.
[36] "*JLC-I*", KEK-Report-92-16 (1992).